Columnar-to-Equiaxed Transition in Solidification Processing of AlSi7 alloys in Microgravity – The CETSOL project

G. Zimmermann[1, a], L. Sturz[1], B. Billia[2], N. Mangelinck-Noël[2], D.R. Liu[2],

H. Nguyen Thi[2], N. Bergeon[2], Ch.-A. Gandin[3], D.J. Browne[4],

Ch. Beckermann[5], D. Tourret[6], A. Karma[6]

[1] ACCESS e.V., 52072 Aachen, Germany;

[2] IM2NP UMR CNRS 7334, Aix-Marseille Universite, 133397 Marseille cedex 20, France

[3] MINES-Paris Tech, CEMEF-ARMINES, F-06904 Sophia Antipolis Cedex, France

[4] University College Dublin, Belfield, Dublin 4, Ireland

[5] University of Iowa, Iowa City, USA

[6] Northeastern University, Boston, USA

[a] g.zimmermann@access-technology.de

Keywords: Solidification, Microgravity, Aluminium-Silicon Alloy, Grain Structure, Columnar-to-equiaxed Transition

Abstract. This paper gives an overview of the experiments on-board the International Space Station (ISS) performed so far by the CETSOL team. Al-7 wt% Si alloys with and without grain refiners were solidified in microgravity. Detailed grain structure analysis showed columnar growth in case of non-refined alloy, but the existence of a columnar to equiaxed transition (CET) in refined alloy. One main result is a sharp CET when increasing the solidification velocity and a progressive CET for lowering the temperature gradient. Applying a front tracking model this behavior was confirmed numerically for sharp CET. Using a CAFE model both segregation and grain structures were numerically modeled and show a fair agreement with the experimental findings.

Introduction

In most casting processes of metallic alloys a competition between the growth of several arrays of dendrites results in characteristic grain structures. Therefore, depending on the process parameters, columnar or equiaxed grain growth or a transition from columnar to equiaxed grains (CET) exists [1-4]. The effect of CET was intensively investigated in the last decades because it's of high relevance in industrial application. Therefore, several computational models of the CET were developed, like volume-averaged models calculating the transport phenomena on the scale of an entire casting [5-7], meso-scale models tracking the growth of the envelope of each individual grain [8-10] or micro-scale and phase field models resolving details of the solid-liquid interface [11, 12]. In spite of the fact that these numerical models are able to describe the CET quite well, there are some shortcomings in the modeling studies. Moreover, in the presence of a gravitational field, settling or floatation of solid particles in the melt and their interaction with the development of the columnar grain structure as well as natural convection of the melt itself must be taken into account in order to predict the grain structure of a casting.

Here, a microgravity environment allows for suppression of buoyancy-driven melt flow and therefore for growth of equiaxed grains free of sedimentation and buoyancy effects. Experiments in microgravity provide unique data for testing fundamental theories of grain structure formation. To carry out such experiments and to model the process of columnar to equiaxed transition is the topic of the research project Columnar-to-Equiaxed Transition in SOLidification Processing (CETSOL) in the framework of the Microgravity Application Promotion (MAP) programme of the European Space Agency (ESA). This programme was initiated more than 10 years ago and continuously driven by scientific teams as well as interested industries from several European countries. In the

last years several solidification experiments were performed successfully in the Low Gradient Furnace insert of the Materials Science Lab (MSL-LGF) onboard the International Space Station (ISS). This paper summarizes main results of these experiments.

Experimental set-up of the microgravity experiments

In microgravity environment, six samples from Al-7wt%Si alloy (refined and non-refined) were processed [13]. The rod-like samples of diameter 7.8 mm and length 245.0 mm were integrated in alumina crucibles. To measure the axial temperature distribution along the sample twelve thermocouples (TC1 to TC12) are located at positions ranging from (TC1) 72.5 mm to (TC12) 182.5 mm in 10 mm distances at the outside of the crucible, defined from the cold end of the samples. A conical shaped Shapal plug acts as passive volume compensation device during heating-up and melting of the alloy. This whole set-up is inserted leak-tight in a tantalum tube filled with 200 mbar helium and is labeled as Sample Cartridge Assembly (MSL-SCA) [13]. For sample processing the MSL-SCA set-up is inserted into the MSL-LGF furnace, which consists of a 'cold zone' with 3 heaters, a 'hot zone' with 4 heaters, separated by an 'adiabatic zone'. By controlling the temperatures of the cold and the hot zone a temperature gradient along the sample axis is applied. Melting and solidification of the metallic alloy is realized by a movement of the furnace insert along the axis of the fixed sample with a defined speed.

The main solidification parameters of the flight experiments are summarized in **Table 1**. In FM1, FM2, FM5 and FM6 refined Al-7 wt% Si alloys with a commercial refiner Al-5wt%Ti-1wt%B were solidified. In FM3 and FM4, non-refined Al-7 wt% Si alloy was chosen. Directional solidification began after different thermal homogenization times [14]. A long homogenization time of 18000 s was used to study the effect of temperature gradient zone melting (TGZM) [15, 16]. In the first solidification phase directional solidification was initiated by raising the pulling velocity of the furnace from 0 mm/s to $v1 = 0.01$ mm/s within a temperature gradient of about 1 K/mm. This phase lasted for 2000 s and was identical for all flight experiments. In solidification phase 2, the temperature of the hot zone was decreased with a cooling rate of -0.067 K/s. This was achieved while keeping unchanged the pulling velocity of the furnace for FM4, FM5 and FM6. In the case of FM1, FM2 and FM3 a velocity jump from $v1 = 0.01$ mm/s to $v2 = 0.20$ mm/s was suddenly induced at the same time as the temperature decrease of the hot zone. Finally, both a shut-down of the heaters and a fast movement of the furnace were applied to complete solidification.

Table 1: Process parameters of the flight experiments

Sample No.	Alloy	Homogenization time	Solidification phase 1		Solidification phase 2			Fast movement
		t_H (s)	$v1$ (mm/s)	$z1$ (mm)	$v2$ (mm/s)	$z2$ (mm)	dT/dt (K/s)	$v3$ (mm/s)
FM1	AlSi7+g.r.	600	0.010	20	0.200	50	-0.067	3.0
FM2	AlSi7+g.r.	18000			0.200	50		
FM3	AlSi7	18000						
FM4	AlSi7	18000			0.010	20		
FM5	AlSi7+g.r.	600			0.010	20		
FM6	AlSi7+g.r.	18000						

Sample Analysis

To analyze the overall quality of the processed samples with respect to porosity or defects non-destructive computer tomography was used. The spatial resolution of about 25 µm allows the reconstruction of a 3D volume model of each sample. As a result only in samples FM1 and FM5, having short homogenization times, some small pores with diameters less than 0.5 mm were detected, which do not influence the solidification behavior significantly.

For analyzing the microstructure and the grain structure the samples were sectioned [13]. First, the samples were cut into pieces of length 30 mm to analyze the transversal cross-sections. Second, each of these pieces was sawed along the axis to get two halves for analysis of the longitudinal cross-sections.

To determine the dendritic microstructure the samples were polished, slightly etched and observed with a microscope. From these longitudinal cross-sections also the distributions of eutectic and dendrite arm spacing (DAS) were analyzed [17]. To identify the grain structure qualitatively the cross-sections were etched electrolytically and analyzed in a polarized light microscope. Then, different colors represent different orientations of the dendritic grains [18]. For quantitative determination of crystallographic orientations of the grains, Electron BackScattered Diffraction (EBSD) patterns were made from selected longitudinal cross-sections. These data were used to evaluate the 3D-crystallographic orientations of the grains with respect to the solidification direction and to evaluate the distributions of sizes and shapes of the grains in the 2D sections.

Results of microgravity experiments with non-refined Al-7wt%Si alloy

Fig. 1 shows maps of the dendritic microstructure and the grain structure in non-refined Al-7wt%Si sample FM3 revealed by electrolytic polishing and polarized-light optical microscopy. The upper row gives radial cross-sections (Q2 – Q4) at different sample positions z. Longitudinal cross-sections L3 and L4 in between Q2 and Q3, and Q3 and Q4 are shown in the lower row. The solidification direction was from left to right.

Cross-section Q2, as well as the left part of longitudinal cross-section L3, shows the polycrystalline mushy zone region. As a result of the long thermal homogenization of 18000 s in a temperature gradient coarsening of the primary Al-rich dendrites exists. Cross-section Q3, as well as the right part of L3 and the left part of L4 reveal competitive growth of columnar dendrites originating from several pre-existing grains in the non-fully melted region according to a solidification with $v1 = 0.01$ mm/s (see Table 1). The increase in the solidification velocity to $v2 = 0.20$ mm/s results in a maintenance of columnar growth but with reduced dendrite spacing. This is demonstrated in cross-section Q4 and in the right part of L4. Detailed analysis shows [17] that in solidification phase 1 a locally high quantity of eutectic correlates with large dendrite arm spacing (DAS). In solidification phase 2, both eutectic quantity and DAS were reduced due to the finer dendritic structure. Additionally, it should be noted that during solidification with $v2 = 0.20$ mm/s, small grains with significant misorientations were found (see Q4). Therefore, despite pure diffusive growth condition some amount of fragmentation exists [17].

Results of microgravity experiments with refined Al-7wt%Si alloy

The recorded cooling curves of the thermocouples TC1 to TC12 are shown in **Fig. 2** for samples FM1 and FM5. The time scale here starts at beginning of the first solidification phase, then at $t = 2000$ s the second phase starts (see Table 1). Additionally, the corresponding furnace positions s are given. For FM1 (and also for FM2) mainly an increase of the solidification velocity from $v1 = 0.01$ mm/s to $v2 = 0.20$ mm/s is expected to trigger CET, whereas for FM5 (and also for FM6) a reduction of the temperature gradient is applied. For further evaluation an averaged interface temperature of 612 °C is used. This takes into account some front undercooling [2] and also the fact that the temperature inside the alloy is somewhat higher than the measured one at the crucible. Such a value was already used in similar microgravity experiments [7].
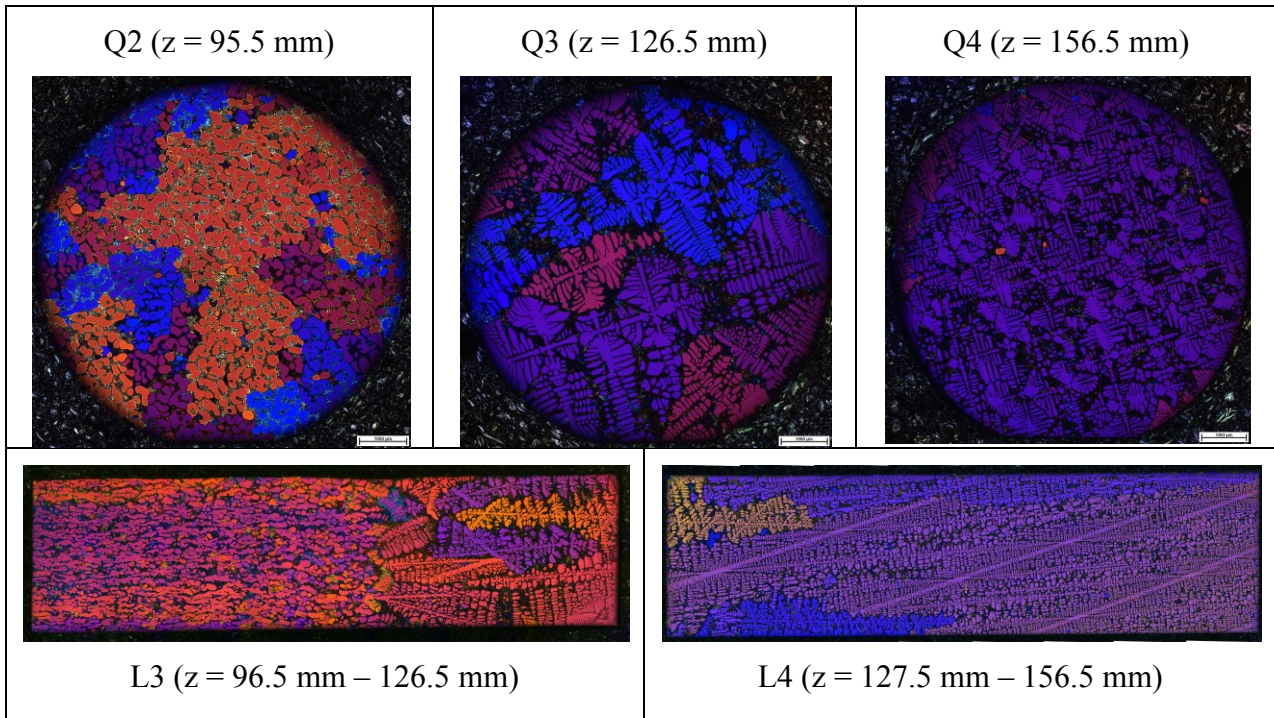
Fig. 1: Maps of the dendritic microstructure and the grain structure in non-refined Al-7 wt% Si sample FM3 revealed by electrolytic polishing and polarized-light optical microscopy, showing radial cross-sections (Q2 – Q4) at given sample positions z and longitudinal cross-sections (L3, L4) in between, with growth direction from left to right.
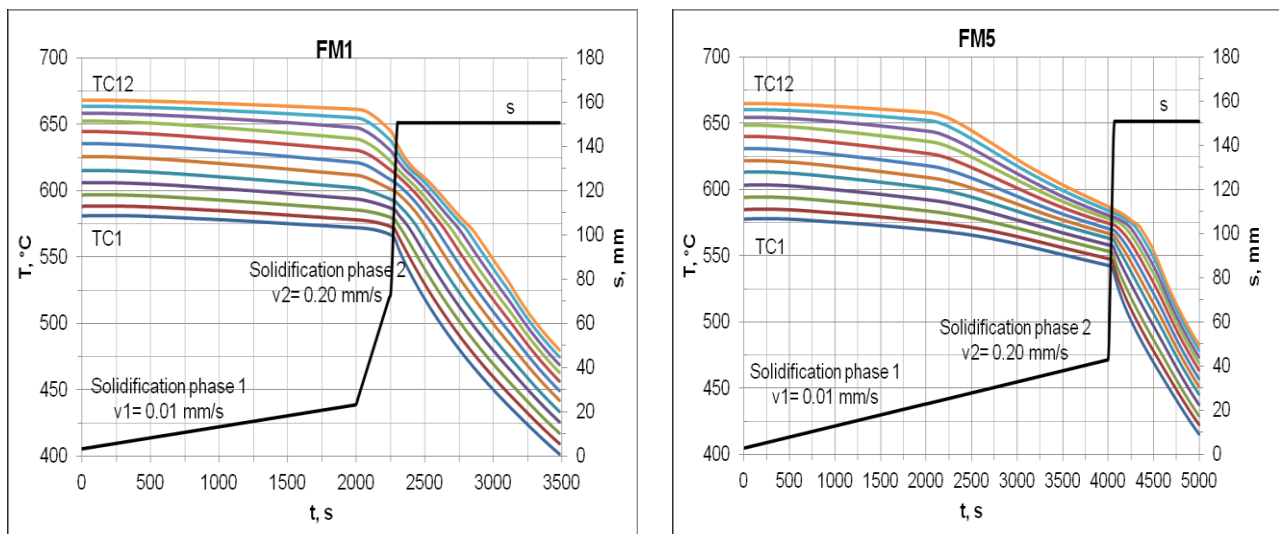

Fig. 2: Measured temperature evolutions at thermocouples TC1 to TC12 and furnace positions s during the solidification phases for samples FM1 and FM5.

Fig. 3 shows the local temperature gradient and velocity of the 612°C-isotherm during the solidification phases for samples FM1, FM2, FM5 and FM6. The values are evaluated at times when the 612 °C-isotherm reaches a thermocouple. At this time the local cooling rate at this thermocouple in a time interval of ± 60 s is determined. Also, from the temperature difference measured between this thermocouple and the closest next thermocouple, knowing the distances between neighboring thermocouples of 10 mm, the temperature gradient ahead of the interface is calculated. From temperature gradient and cooling rate the local isotherm velocity is determined (Fig. 3).
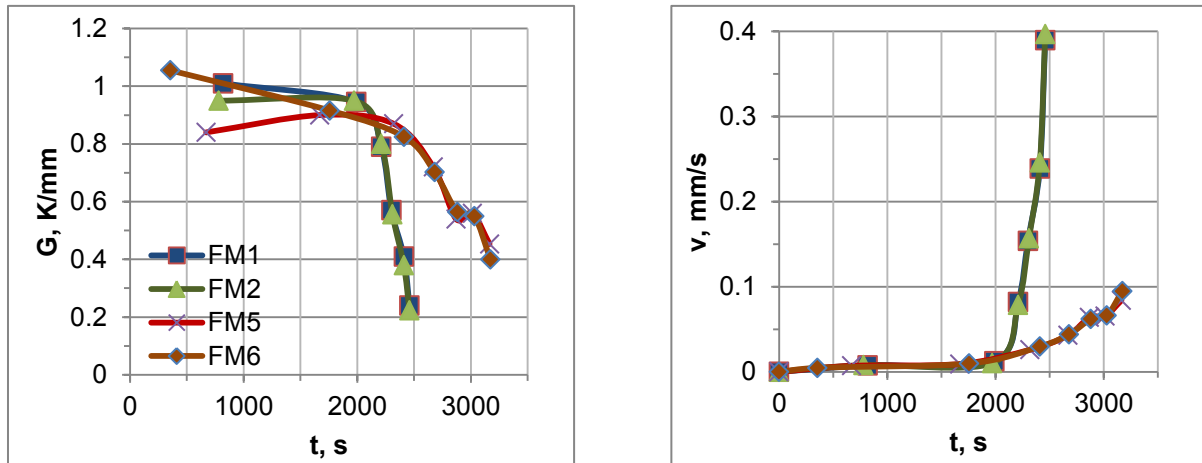
Fig. 3: Local temperature gradient and isotherm velocity during solidification phases for samples FM1, FM2, FM5 and FM6 (t = 0 s corresponds to the beginning of furnace movement with v1 = 0.01 mm/s and at t = 2000 s starts solidification phase 2)

The temperature gradient is nearly constant at G = 0.95 ± 0.1 K/mm in the first solidification phase with v1 = 0.01 mm/s. In experiments FM1 and FM2 a second solidification phase with a furnace movement of v2 = 0.20 mm/s and a simultaneous cooling down of the heater temperatures with 0.067 K/s for 250 s followed. In this phase a slight decrease of the temperature gradient to about 0.6 K/mm is measured. A further decrease is related to the "fast movement" (see Table 1). In experiments FM5 and FM6 a second solidification phase with an unchanged furnace velocity for another 2000 s and a simultaneous cooling down of the heater temperatures with 0.067 K/s was applied (see Table 1). In this phase a smooth decrease of the temperature gradient to about 0.5 K/mm exists before the sample is completely solidified. A qualitatively similar behaviour is determined for the local interface velocity. In the second solidification phase in experiments FM1 and FM2 the velocity reaches about the value v = 0.20 mm/s, given by the furnace movement. In experiments FM5 and FM6 the increase is much lower.

Fig. 4 shows maps of the grain structure in refined Al-7 wt% Si samples FM1, FM2, FM5 and FM6 identified by electrolytic polishing and polarized-light optical microscopy. The longitudinal cross-sections (L4) reveal the transition region from columnar growth (left part of each cross-section) to equiaxed growth.
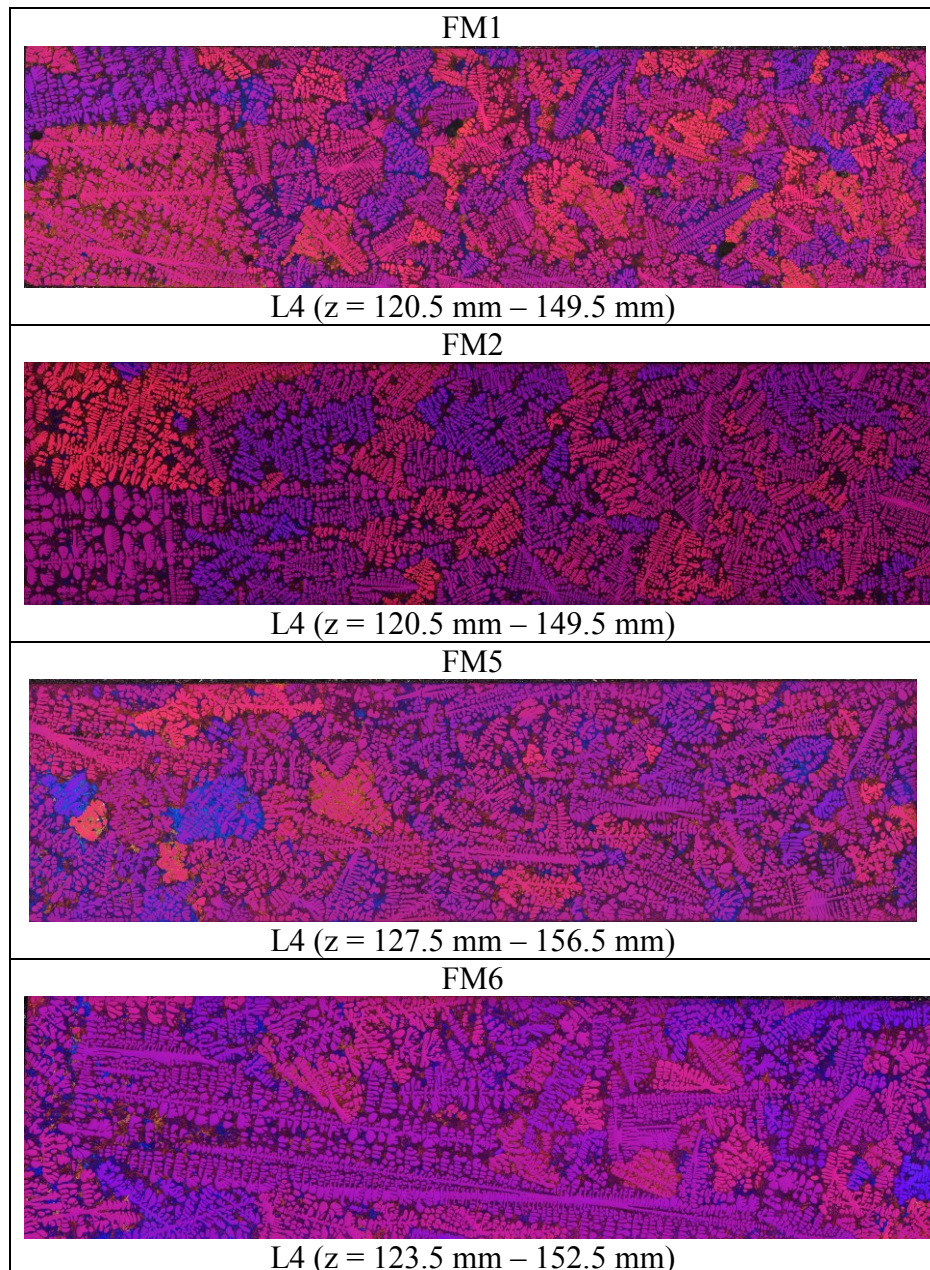
Fig. 4: Maps of the grain structure in refined Al-7wt% Si samples FM1, FM2, FM5 and FM6 showing the transition region from columnar (left part of the cross-sections) to equiaxed growth in the longitudinal cross-sections (L4).

For quantitative analysis of CET the grain structure in the longitudinal cross-sections L4 was also determined using EBSD measurement. **Fig. 5** shows the misorientation of the crystallographic (100) axis of each grain with respect to the sample axis, which also correspond to the direction of solidification (here from left to right). The grey level is related to the misorientation angles. Black color means no misorientation (0°), whereas white color belongs to maximum misorientation (54.74°). The orientation maps indicate a sharp transition from columnar growth with two grains to many equiaxed grains with fully random orientations in the cross-section L4 of FM2, and a rather smooth transition in case of FM6.

For further evaluation of the CET the size of the grains in L4 and L5 longitudinal cross-sections were evaluated. **Fig. 6** shows the average grain size in intervals of ± 2 mm. Samples FM1 and FM2 show a sharp transition from large grain sizes to low ones at $z = 127 \pm 2$ mm and $z = 126 \pm 2$ mm, respectively. The grain size changes significantly by a factor of about 5. Therefore, these positions are defined as the beginning and end positions for CET for FM1 and FM2 samples (see also Table 2). **Fig. 6** also shows the average grain size of samples FM5 and FM6. The difference between both curves can be traced back

FM2

L4 (z = 120.5 mm – 149.5 mm)

FM6

L4 (z = 123.5 mm – 152.5 mm)

Fig. 5: Misorientation of the crystallographic (100) axis of each grain with respect to the sample axis in the longitudinal cross-sections L4 of samples FM2 and FM6. The grey scale is related to the misorientation angles from 0° (black) to maximum value 54.74° (white).

to one rather large grain in FM6 (see Fig. 5). First, a more continuously decrease of the averaged grain size is detected, followed later by a halving of the grain size. The beginning and the end of this descent of the averaged grain size can be identified as the beginning and end positions for CET (see also Table 2).

Another indicator for CET is the elongation factor of the grain structure, which is defined by the ratio of the length of the major axis to the length of the minor axis of each grain, intersecting orthogonally at the centroid of the grain. In Liu et al. [17] the grain structure is labeled 'equiaxed' in case the elongation factor is lower than 2 according to considerations developed by Hunt [19]. Analysis of FM5 shows that the averaged elongation factor stays above 2 up to about $z = 156$ mm [17]. Therefore, this position corresponds well with the end position for CET determined by the analysis of the grain size.
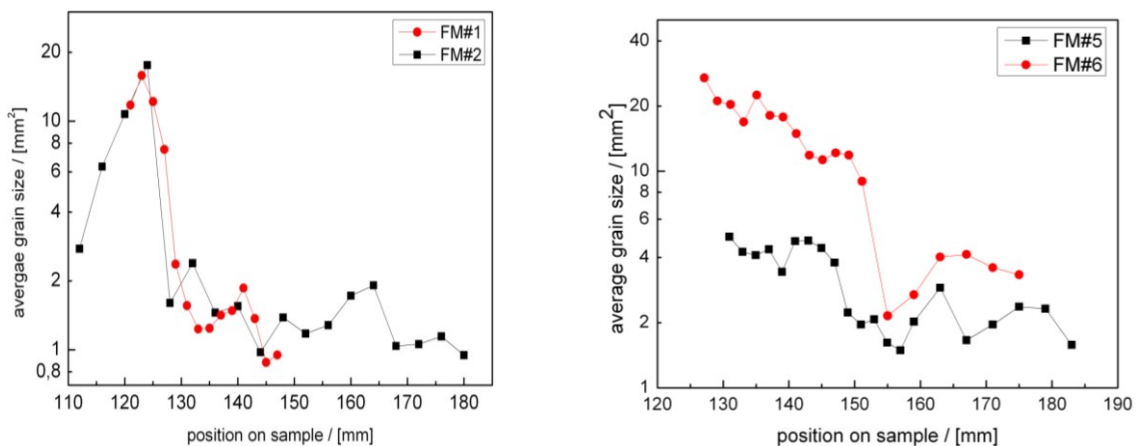

Fig. 6: Average grain size in L4 and L5 longitudinal cross-sections. Samples FM1 and FM2 show a sharp transition; FM5 and FM6 a rather smooth transition.

The CET-positions for all samples are summarized in **Table 2**. Also the CET-positions normalized to the initial solid-liquid interface position at $t = 0$ s are given. Within the measurement error the beginning positions for CET in all samples are the same ($z = 55 - 57$ mm), whereas the end positions depend of the type of CET, either sharp ($z = 60 - 61$ mm), or progressive ($z = 83$ mm).
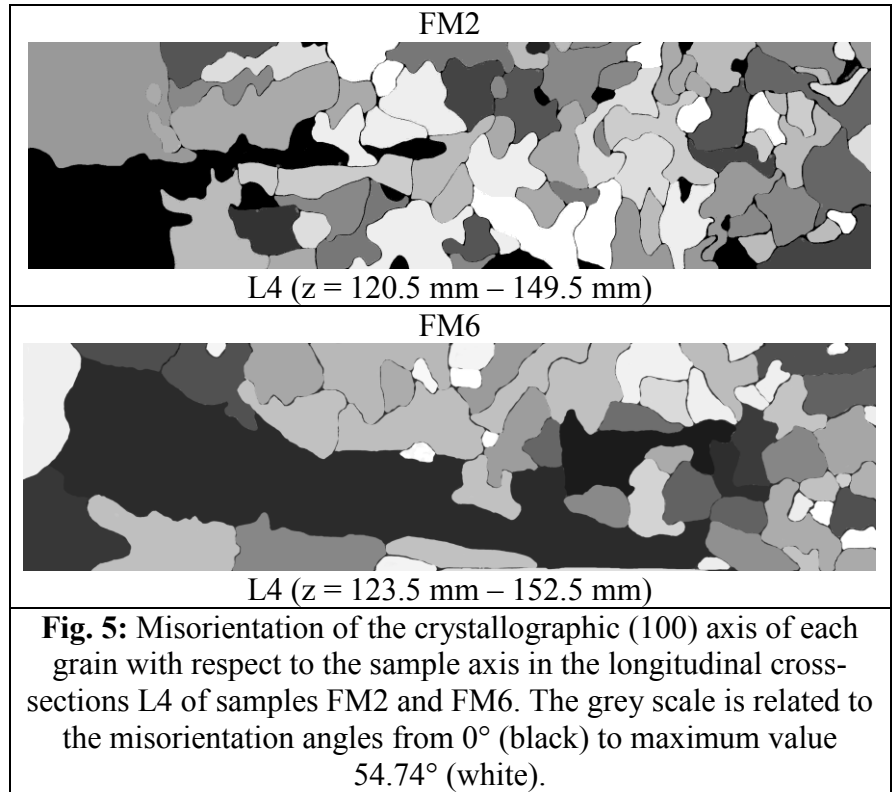
Table 2: CET positions

	FM1	FM2	FM5	FM6
	sharp CET		progressive CET	
CET-position, mm	125 - 129	124 - 128	130 - 156	126 - 154
Initial s/l-position, mm	68	68	73	71
Normalized CET-position, mm	57 - 61	56 - 60	57 - 83	55 - 83

The major reason responsible for this progressive CET in FM5 and FM6 is the low pulling velocity of v1 = 0.01 mm/s. Newly nucleated grains in the undercooled melt grow a relatively long distance before the maximum undercooling in front of the tips reaches the critical nucleation temperature necessary for the nucleation of new grains. If gradually repeated nucleation events predominate, an intermediate zone with a coexistence of elongated and equiaxed grains forms which postpones the CET [17]. At CET, a fast repeated nucleation of grains exists which competes over the continued growth of existing grains to form a truly equiaxed zone [20].

Numerical modelling

The experimental results obtained from the microgravity experiments are used for development and improvement of numerical modelling.

An approach that combines front tracking of columnar growth and an equiaxed volume averaging method was employed to simulate both the FM2 and FM3 experiments. In FM2 sample the possibility of equiaxed nucleation from grain refiners in the undercooled liquid ahead of the advancing columnar front is considered. The CET position is predicted at a distance z = 127.5 mm, which corresponds rather well with the experimental value of z = 124 - 128 mm. In the non-refined sample FM3 however, no CET was found, both in the simulations and in the experiment. Further details have been published in [13, 14 and 21].

Axi-symmetric simulations also were carried out using two-dimensional cellular automaton - finite element modeling [22, 23]. Modelling of nucleation and growth of the grain structure is performed together with segregation. **Fig. 7** shows the simulated grain structure of experiments FM1 and FM5, using refined alloys. In that case, the same values of the nucleation parameters are used for all simulations, i.e. Gaussian distribution of the heterogeneous particles with an average undercooling of 4 °C, a standard deviation of 0.5 °C and a maximum density of $5 \cdot 10^{10}$ m^{-3}. As a consequence, the differences in CET are only due to the solidification conditions. The occurrence of a columnar zone at the beginning of solidification phase 1 is observed, followed by the nucleation of new grains and the formation of an equiaxed zone. The simulated equiaxed grain density increases with the cooling rate. The grain structure evolution in both experiments is well retrieved by the simulations and also confirms the type of CET, sharp or progressive.
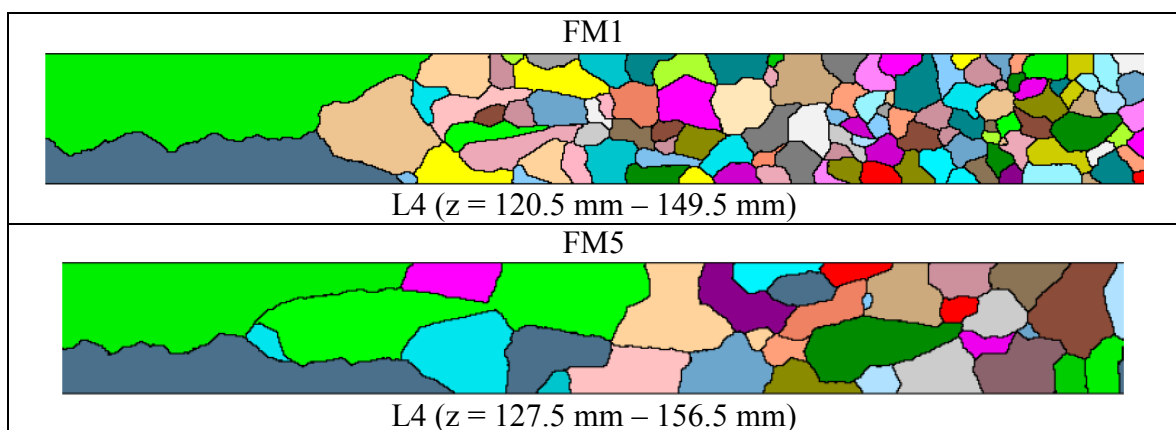

Fig. 7: Simulated grain structures in longitudinal cross sections L4 of FM1 (top) and FM5 (bottom) showing sharp and progressive CET for comparison with experimental structures given in Figure 4.

Conclusion

This paper gives an overview of the experiments performed so far on-board the International Space Station (ISS) by the CETSOL team. In the Materials Science Laboratory, Al-7 wt% Si alloys with and without grain refiners were solidified in diffusive conditions. Detailed grain structure analysis showed columnar growth in case of non-refined alloy, but the existence of a columnar to equiaxed transition in refined alloy. Main result is a sharp CET when increasing the solidification velocity and a progressive CET for lowering the temperature gradient. Applying a front tracking model this behavior was confirmed numerically. Using a CAFE model both segregation and grain structures, as well as CET, were numerically modeled and show a fair agreement with the experimental findings. In future, more experiments on-board the ISS will be performed with different process parameters to broaden the data basis. In parallel, numerical 3D-modeling of grain growth is in progress [24, 25].

Acknowledgements

References

[1] J.D. Hunt, A numerical analysis of time dependent isolated dendritic growth for conditions near the steady state, Acta Metall. Mater. 38 (1990) 411-418.

[2] Ch.-A. Gandin, From constrained to unconstrained growth during directional solidification, Acta Mater. 48 (2000) 2483-2501.

[3] D.J. Browne , J.D. Hunt, A fixed grid front-tracking model of the growth of a columnar front and an equiaxed grain during solidification of an alloy, Numerical Heat Transf., Part B: Fundamentals 45 (2004) 395-419.

[4] L. Sturz, G. Zimmermann, Investigations on Columnar-to-Equiaxed Transition in Binary Al Alloys with and without Grain Refiners, Materials Science Forum 508 (2006) 419-424.

[5] M.A. Martorano, C. Beckermann, Ch.-A. Gandin, A solutal interaction mechanism for the columnar-to-equiaxed transition in alloy solidification, Met. Mat. Trans. 34A (2003) 1657-1674.

[6] A. Ludwig, M. Wu, Modeling the columnar-to-equiaxed transition with a three-phase Eulerian approach, Mater. Sci. Eng. A413-414 (2005) 109-114.

[7] A. Noeppel, O. Budenkova, G. Zimmermann, L. Sturz, N. Mangelinck-Noël, H. Jung, H. Nguyen-Thi, B. Billia, C.-A. Gandin, Y. Fautrelle, Numerical modelling of columnar to equiaxed transition – application to microgravity experiments, Int. J. Cast Metals Research 22 (2009) 34-38.

[8] Ch.-A. Gandin, M. Rappaz, A coupled finite element-cellular automaton model for the prediction of dendritic grain structures in solidification processes, Acta Metall. Mater. 42 (1994) 2233-2246.

[9] P. Delaleau, C. Beckermann, R.H. Mathiesen, L. Arnberg, Mesoscopic Simulation of Dendritic Growth Observed in X-ray Video Microscopy During Directional Solidification of Al–Cu Alloys, ISIJ International 50 (2010) 1886-1894.

[10] J. Banaszek, S. McFadden, D.J. Browne, L. Sturz, G. Zimmermann, Natural Convection and Columnar-to-Equiaxed Transition Prediction in a Front-Tracking Model of Alloy Solidification, Met. Mat. Transact. A38 (2007) 1476-1484.

[11] H.B. Dong, P.D. Lee, Simulation of the columnar-to-equiaxed transition in directionally solidified Al–Cu alloys, Acta Mater. 53 (2005) 659-668.

[12] A. Badillo, C. Beckermann, Phase-field simulation of the columnar-to-equiaxed transition in alloy solidification, Acta Mater. 54 (2006) 2015-2026.

[13] G. Zimmermann, L. Sturz, B. Billia, N. Mangelinck-Noël, H. Nguyen Thi, Ch.-A. Gandin, D.J. Browne, W.U. Mirihanage, Investigation of columnar-to-equiaxed transition in solidification processing of AlSi alloys in microgravity – The CETSOL project, J. of Physics: Conference Series 327 (2011) 012003

[14] W.U. Mirihanage, D.J. Browne, G. Zimmermann, L. Sturz, Simulation of international space station microgravity directional solidification experiments on columnar-to-equiaxed transition, Acta Mat. 60 (2012) 6362-6371.

[15] H. Nguyen Thi, B. Drevet, J.M. Debierre, D. Camel, D.B. Yao, B. Billia, Preparation of the initial solid–liquid interface and melt in directional solidification, J. Cryst. Growth 253 (2003) 539-548.

[16] H. Nguyen Thi, G. Reinhart, A. Buffet, T. Schenk, N. Mangelinck-Noël, H. Jung, N. Bergeon, B. Billia, J. Härtwig, J. Baruchel, In situ and real-time analysis of TGZM phenomena by synchrotron X-ray radiography, J. Cryst. Growth 310 (2008) 2906-2914.

[17] D. R. Liu, N. Mangelinck-Noël, Ch.-A. Gandin, G. Zimmermann, L. Sturz, H. Nguyen Thi, B. Billia, Structures in directionally solidified Al–7wt.%Si alloys: Benchmark experiments under microgravity, Acta Materialia 64 (2014) 253-265.

[18] E. Schaberger, F. Grote, A. Schievenbusch, Farbätzung und Farbbildanalyse - Ein Weg zur Charakterisierung von Gefügen innovativer Gusswerkstoffe, Prakt. Metallographie 37 (2000) 419-434.

[19] J.D. Hunt, Steady state columnar and equiaxed growth of dendrites and eutectic, Materials Science and Engineering 65 (1984) 75-83.

[20] M. Vandyoussefi, A.L. Greer, Application of cellular automaton–finite element model to the grain refinement of directionally solidified Al–4.15 wt% Mg alloys, Acta Mater. 50 (2002) 1693-1705.

[21] W.U. Mirihanage, D.J. Browne, L. Sturz, G. Zimmermann, Numerical Modelling of the Material Science Lab - Low Gradient Furnace (MSL-LGF) Microgravity Directional Solidification Experiments on the Columnar to Equiaxed Transition, IOP Conference Series: Materials Science and Engineering 27 (2011) 012010

[22] S. Mosbah, M. Bellet, Ch.-A. Gandin, Experimental and Numerical Modeling of Segregation in Metallic Alloys, Met. Materials Transactions 41 (2010) 651-669.

[23] Ch. A. Gandin, Modeling of solidification: Grain structures and segregations in metallic alloys, Modélisation deCompte rendus physique 11 (2010) 216-225.

[24] T. Carozzani, H. Digonnet, Ch.-A. Gandin, 3D CAFE modeling of grain structures: application to primary dendritic and secondary eutectic solidification, Modeling and Simulation in Materials Science and Engineering 20 (2012) 015010.

[25] T. Carozzani, Ch.-A. Gandin, H. Digonnet, M. Bellet, K. Zaidat, Y. Fautrelle, Direct Simulation of a Solidification Benchmark Experiment, Met. Mater. Transact. A44 (2013) 873-887.